-RESEARCH PAPER-

International Journal of Mining and Geo-Engineering

IJMGE

IJMGE 56-4 (2022) 349-359

DOI: 10.22059/IJMGE.2022.339663.594953

Physical model simulation of block caving in jointed rock mass

Behnam Alipenhani [a], Hasan Bakhshandeh Amnieh [a, *], Abbas Majdi [a]

[a] *School of Mining Engineering, College of Engineering, University of Tehran, Tehran, Iran.*

Article History:

Received: 25 February 2022.

Revised: 01 May 2022.

Accepted: 21 May 2022.

ABSTRACT

Incorrect estimation of undercut dimensions in the block caving method can lead to the cessation of caving operations and loss of a large portion of deposits. Numerical modeling is one of the methods for determining the minimum caving span. Numerical and physical modeling methods are useful for an accurate understanding of caving operations. Accordingly, this research focused on investigating the performance of physical and numerical modeling in determining the effects of depth and joint orientation on the minimum required caving span for the initiation and propagation of caving. The physical model was made with 1.5*1.5 square meter dimensions and consisted of travertine blocks with 4*4 square centimeter dimensions. In addition, joints were modeled with dips of 0, 90, 45, 135, 30, and 120 degrees. The physical model could simulate ground stress conditions to great depths and show the behavior of the jointed rock mass in a two-dimensional space. Further, by capturing this behavior, it was possible to compare its result with UDEC software. The results demonstrated that the number of falling blocks and the height of the caving increased by increasing the dip. Furthermore, the formation of arches due to high horizontal stress stops the caving, which will occur again with the increasing span. Although the horizontal stresses and geometrical properties of the joints affect the shape of the caving area, its shape largely follows the dip and orientation of the rock mass joints. Poor draw control causes caved ore columns, which can lead to the formation of a stable arc. Finally, the height of the caved back increases in each span by increasing the depth while decreasing the dip of the joints.

Keywords: *Block caving, Caving span, Physical modeling, Numerical modeling, UDEC.*

1. Introduction

An accurate understanding of the process that occurs at the initiation and propagation of caving helps determine the cavability of the rock mass. As stated by Laubscher [1] and Chitombo [2], block caving operations are now moving toward super-caves. Caving will stop if the undercut dimensions are insufficient for its initiation and propagation; in addition, much of the orebody will be lost, and additional costs must be incurred to re-induce caving.

Many studies have focused on the cavability assessment of rock mass from analytical, empirical, numerical, and physical modeling viewpoints. Tables 1 and 2 present the history of the performed studies in this field

Numerical modeling is used to predict cavability; however, the results depend on the accuracy of the input data. Thus, a better understanding of the caving process is needed to calibrate numerical models. The physical modeling of caving helps perform numerical modeling and is highly useful to ensure the accuracy of predictions about caving in different mines [2]. The three-dimensional (3D) physical model of caving is extremely challenging, requires extensive time and cost, and is even impossible to perform due to its extremely large scale. It is noteworthy that the physical modeling of caving is possible in two dimensions.

Cumming-Potvin and Wesseloo [32] and the Itasca research group used a geotechnical centrifuge to accelerate the physical model of gravity to g80. Based on the Hoek Scale [32], the experiment represents a state several times the actual size of the sample by accelerating the Earth's gravity. The experiments were 2D, and an on-screen DSLR camera facilitated the observation of the demolition behavior. These experiments showed that the propagation of caving could occur through a series of fractures parallel to the surface of the caving and progress as a "jump" to parallel and vertical failure. In this paper, this mechanism is called 'fracture banding'.

Physical modeling was performed by Jacobsz and Kearsley [33] at the University of Pretoria in South Africa to investigate the mechanism of caving propagation in large-scale mines. The experiment was conducted on a weak artificial rock mass with high and low horizontal stress conditions, and it was found that in the experiment, rock fracture occurred by fracture banding. This is different from Duplancic's [22] conceptual model, which is typically accepted as a model for describing processes associated with caving propagation. Fracture banding demonstrates a series of jumped fractures parallel to the cave-back, which is in contrast with the conceptual model of Duplancic [35]. The differences in the profile damage of the continuous and banding fracture models are schematically illustrated in Figure 1. The results of the above-mentioned experiment also revealed that the initial fractures and cracks of the model control the extent of caving propagation.

Similarly, Bai et al [34] conducted physical modeling to find a suitable structural material that can represent the process of top coal caving. In their study, a series of experiments were performed on two large-scale physical models, including sand, gravel, gypsum, and mica to evaluate the cavability of the top coal with hard rock bands based on two real cases. The results of these experiments indicated that the embedded hard rock bands in the top coal caused poor crushing and low cavability, the quality of which also depends on the strength, thickness, and location of the hard rock bands. Moreover, based on the results of these experiments, the amount of the fragmented zone can be used as the main parameter that reflects all factors affecting the cavability in the top coal [34].

* Corresponding author: *Fax:* 021-88008838, *Tel:* 021-82084141, *E-mail address:* hbakhshandeh@ut.ac.ir (H. Bakhshandeh Amnieh).

Table 1. History of analytical, empirical, and numerical methods used for cavability assessment.

Model type	References	Purpose and application
Analytical	Rice and Panek (1948) [3]	Providing a simple 1D volumetric method to investigate the caving propagation behavior by assuming constant coefficients of volume increase.
	Ross et al. (2005) [4]	Estimation of caving propagation rates at the Northparkes mine in Australia.
	Carlson et al. (2008) [5]	Estimation of caving propagation rates at Henderson mine, Colorado, USA.
	Beck et al. (2011) [6]	Estimation of caving propagation rates at ridgeway deeps mine, Australia.
	Someehneshin et al. (2015) [7]	Determination of the optimal block size in the block caving method by the analytical method.
Empirical	King (1945) [8]	Estimation of rock mass cavability based on the rock type, discontinuities spacing, and mineralogy.
	McMahon (1969) [9]	Presentation of the cavability index (CI) to predict the cavability, fragmentation, and secondary blasting requirements using the data from the Climax and Urad mines and establishing a relationship between CI and RQD.
	Morison (1976) [10]	Providing a qualitative procedure for selecting the extraction methods in hard rocks.
	Laubscher (1981) [11]	Providing a procedure for selecting the underground mass mining method based on the minimum span.
	Laubscher (1990) [11]	Presentation of hydraulic radius diagram in MRMR by combining the caving mine data
	Mathew et al. (1980) [12]	Presenting a hydraulic radius graph in terms of stability number by combining the caving mine data.
	Potvin et al. (1980) [13]	Adding the data to the Mathews graph and modifying the stability graph.
	Stewart (1980) [13]	Adding the data to the Mathews graph and modifying the stability graph.
	Trueman (2000) [14]	Development of the data related to stability, minor and major failures of the studied areas, and application of the Mathews method in a wide range of rock mass characteristics.
	Mawdesley (2003) [15]	The method of predicting the spontaneous propagation of caving through the stope stability graph.
	Mime et al. (2008) [16]	Combining the Mathews graph with the dilution diagram data related to the design of the hanging wall of an open stope.
Numerical (Distinct Element)	Lorig et al. (1995) [17]	Using the PFC2D code to better understand the in-situ fracture and improved shape of the cave back.
	Brown (2003) [18]	Demonstrating the capacity of the discrete element method to simulate both the caving initiation mechanisms in a jointed rock mass (stress and gravity).
	Gilbride et al. (2005) [19]	Evaluation of subsidence at the Questa mine using PFC3D.
	Kalenchuk (2008) [20]	Prediction of dilution in sub-level caving mine at Ekati Diamond.
	Zhao et al. (2009) [21]	Simulation of the caving process in the TOP coal method using PFC2D.
	Sharrock et al. (2011) [22]	Modeling caving mechanisms in the large-scale subsidence analyzes.
	Gao et al. (2014) [23]	Modeling of progressive caving of layers on top of coal mining panel by the long wall method using UDEC.
	Rafiee et al. (2018) [24]	Investigating the effect of 7 different parameters on cavability using the SRM technique.
	Song et al. (2019) [25]	Numerical modeling based on 3D particles for process simulation (LTCC).
	Wang et al. (2020) [26]	Investigating the effect of top coal block size on the caving mechanism.
	Alipenhani et al. (2022) [27]	Determination of caving hydraulic radius of rock mass in block caving method using numerical modeling and multivariate regression.

Table 2. History of other methods used in cavability assessment.

Model type	References	Purpose and application
Physical modeling	Park and Kicker (1985) [28]	Study of the stress distribution around chain pillar in the long wall method.
	Whittaker *et al.* (1985) [29]	Study of mining-induced subsidence by the long wall method, and investigation of the fractures at the upper floors of the stope.
	McNEARNY and ABEL (1993) [30]	Study of draw behavior of jointed rock mass in the block caving method.
	Carmichael and Hebblewhite (2012) [31]	Analysis of crack propagation and the areas formed in the large caving extraction method.
	Potvin (2016) [32]	Analysis of the caving mechanism under the plane strain conditions in a centrifuge experiment.
	Jacobsz and Kearsley (2018) [33]	In a centrifuge experiment, the results of placing a weak mass of artificial rock under high and low horizontal stress conditions were examined.
	Bai *et al.* (2018) [34]	In this study, experiments were performed on two large-scale physical models including sand, gravel, gypsum, and mica to investigate the cavability of top coal with hard rock bands based on two real cases.
	Khosravi *et al.* [35]	Investigation of the caving mechanism in the block caving method using numerical and physical modeling.
Fuzzy rock engineering system	Rafiee *et al.* (2016) [36]	Investigation of the effective factors on cavability using the fuzzy system.
Rock engineering system	Azadmehr *et al.* (2019) [37]	Estimation of rock mass cavability in the mass caving method using the RES engineering systems method.
	Rafiee *et al.* (2015) [38]	Investigation of the factors affecting cavability using a rock engineering system (RES)
Probabilistic	Mohammadi *et al.* (2020) [39]	Presenting a probabilistic model for estimating the minimum caving span in the long wall method.

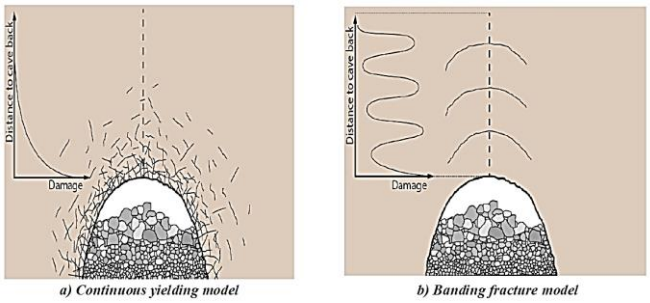

Figure 1. Illustration of damage profile conceptual models [33].

Likewise, Castro et al [40] applied an experimental solution using a scaled model to examine the role of a draw policy on induced vertical stresses in a block-caving layout. They studied isolated, panel caving, and block caving draw policies and concluded that induced vertical stresses are in the range of 0.3 and 2.8 times their initial vertical values and strongly rely on the distance from the extraction front and the dimension of the draw and non-draw areas. These results present useful information for designing a support system in block or panel caving exploitation methods to decrease induced vertical stresses and define extraction guidelines to avoid the hazards of overstressing that can be expected on production-level pillars [40].

The current research aims to perform physical model tests to assess the effects of the number of joint sets, dip of the joint set, and depth on the minimum required caving span. A vertical platform is used to test the rock mass model formed by the rectangular blocks of Travertine.

In the first model, a rock mass with two joint sets perpendicular to each other is simulated, which is 1.5 meters high under the weight of the block itself. In the second model, the same conditions are considered with a dip of 45 and 135. Additionally, three joint sets with a dip of 30 and 120 degrees (two joint sets intersecting) and under the gravity stress of 2.5 MPa were simulated in the third model. The horizontal and vertical joint spacings were 4 cm. The cavability test results are compared with those simulated from discrete element analyses using the discrete element method (DEM) method. The schematic flowchart of the methodology is depicted in Figure 2.

2. Test platform

The frame of the applied physical model for simulating the caving process of the jointed rock mass had four main parts, including an outer steel frame 2 * 2.2, an inner steel frame movable on rails, the lower structure for creating the undercut, and the hydraulic jack for loading the gravitational stress (Figure 3). The inner steel frame, in front of which the Plexiglas sheet is placed, has the ability to place stone blocks with a thickness of 5 cm up to a height of 2 meters. A hydraulic jack with a capacity of 60 tons was considered to apply vertical pressure in the center of the upper part. The jack piston passes through the space between the two upper beams and forces the 50 mm steel strap located on the last row of blocks. The rigidity of this strap causes a uniform force to be applied to the stone blocks. In addition, four 30 mm screws were used to apply horizontal stress in the new system. The front view of the device, in which the blocks are placed, is displayed in Figure 1. Due to the existing limitations, it was decided to increase the span by 4 cm steps. Accordingly, the foundations of stone blocks with a width and height of 50 cm were laid from the ground to the bottom of the model groove. Thus, a 4 cm undercut was made by removing each of these bases (Figure 4). It is noteworthy that the blocks arranged from the front and back must be restricted to create a plane strain mode in the model.

To this end, Plexiglas was employed on the front to facilitate photographing the model's behavior, and three pieces of steel plate with a thickness of 2 mm were applied on the back. The low friction between Plexiglas and the blocks and the distance of about 1 mm between the steel plates and the blocks cannot prevent the natural collapse of the blocks. Three-piece steel plates allow the arrangement of stone blocks at three consecutive heights of 50 cm and are screwed together.

After finishing the arrangement of the blocks, the back plates are placed in their place. The side screws are rotated to apply lateral pressure and establish a zero-displacement condition. Further, the axis of the camera is placed in the center of the model. To create the undercut, the pillars were sequentially removed by moving the pillar from the center, leading to the creation of an undercut with a width of 4 cm. This continues until removing all the pillars. Due to the open space under the frame, the fallen blocks can be drawn as follows.

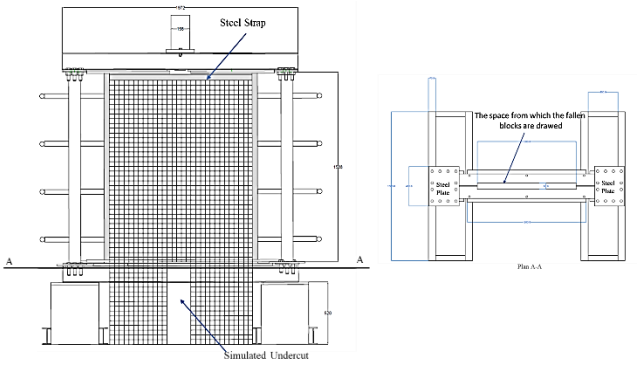

Figure 3. (a) Schematic diagram of the physical model frame and (b) Example of an actual physical model test.

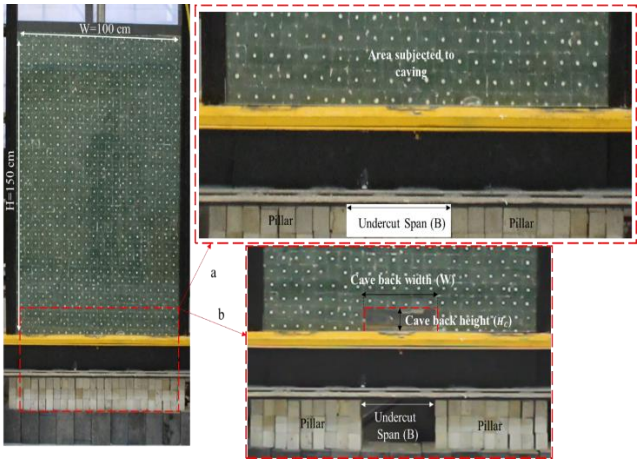

Figure 4. Typical model characteristics and parameter definition: (a) Prepared model and (b) Failure occurring due to undercutting.

3. Rock sample

Travertine from the Khoy quarry mine was used to prepare the tested block specimens, and micritic limestone was the sample. The main constituent minerals of this rock are quartz, microcrystalline calcite, and dolomite. The amount of quartz mineral is less than 5%, and the average density is 2.35 gr/cm3. Cubic travertine blocks with dimensions of 4 × 4 × 5 cm were employed to create the joint. The properties of intact rock and joints are required for numerical modeling and the study of the rock behavior applied for physical modeling. For this purpose, several stone blocks were prepared from the Khoy quarry mine. In the Rock Mechanics Laboratory of the University of Tehran, various samples were prepared for the uniaxial compressive test (ASTM D7012), indirect tensile strength (ASTM D3967) direct shear (ASTM D5607) of the joint surface, and Schmidt hammer (ASTM D5873).

The stress-strain curve of one of the samples is shown in Figure 5, and the test results of the mechanical properties of the samples are provided in Table 3.

The stress level of the model must be determined for evaluating the rigidity of the samples used in the physical model. The maximum pressure on the model is applied when considering the total capacity of the jack (60 tons). At the height of 150 cm and the width of 100 cm of the model and the 5 cm width of the travertine blocks, the maximum stress applied to the lower blocks equals 11.52 MPa. Based on the obtained values from the experiment at the stress of 37.56, the length reduction is about 0.102 mm. The length reduction will be linear because the sample is in an elastic state at this stress. At the stress level in the physical model (11.52 MPa), the length change will be 0.03 mm, which can be easily ignored, thus the prepared travertine blocks will have no problem in terms of rigidity.

To determine the surface characteristics of the blocks, direct shear and Schmidt hammer tests were performed, the results of which are shown in Figures 6 and 7 and Table 4.

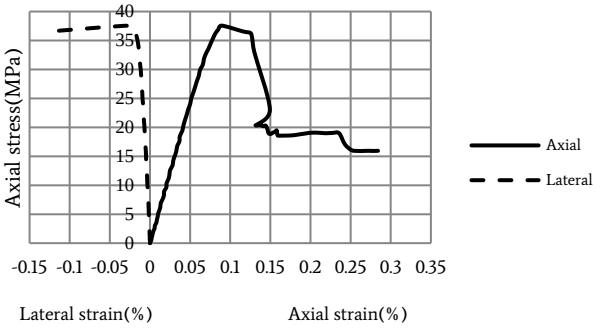

Figure 5. Stress-strain curve from a uniaxial compressive test of Travertine.

Table 3. Mechanical properties of Travertine.

Test number	Tensile strength (MPa)	Uniaxial compressive strength (MPa)	Poisson ratio	Modulus of elasticity (GPa)
1	5.97	45.2	0.13	48.72
2	5.86	34.59	0.18	40.83
3	4.96	32.61	0.15	42.83
4	6.02	26.38	0.14	45.63
5	5.75	33.49	0.15	46.73
6	5.89	37.38	0.18	44.5
7	5.68	38.72	0.14	48.82
8	5.77	42.22	0.15	48.67
9	6.6	45.36	0.13	49.39
10	5.5	37.56	0.18	48.47
Average	5.8	37.35	0.15	46.5

To determine the surface characteristics of the blocks, direct shear and Schmidt hammer tests were performed, the results of which are shown in Figures 6 and 7 and Table 4.

To measure normal stiffness, first, the joints are loaded to half of the uniaxial compressive strength of the intact rock and then unloaded, followed by repeating the same procedure for the intact rock. The difference between the obtained values from the vertical stress-vertical displacement diagram of the rock joint with the intact rock diagram (Figure 8) has a linear trend whose slope equals the normal stiffness of the joint surface [41]. The result of this experiment is illustrated in Figure 9.

4. Physical model testing

Physical modeling must have established rules of similarity in terms of geometric, boundary conditions, physical and mechanical properties, and stress conditions [42,43]. The theory requires that some similarity coefficients, defined as the ratios of prototype parameters for modeling parameters, must be constants [44,45]. The optimal geometric scale factor was taken to be 0.01 based on experts' opinions and economic issues. Selecting a smaller scale makes it difficult to model the joints. In addition, choosing a larger scale requires much money to build frames and power equipment. To simplify the task, in situ rock mass materials were assumed for use. Scale factors are listed in Table 5. The conditions in the physical model can be attributed to an actual condition by these scale factors.

As mentioned earlier, this experiment primarily sought to identify the initiation and propagation of caving, and image analysis was employed for this purpose. The experimental process was imaged to investigate the behavior of the caving rock mass. Then, the captured videos were converted into photos and underwent analysis.

The experiments were performed by preparing the travertine blocks for image analysis. To this end, only photographing and measuring the

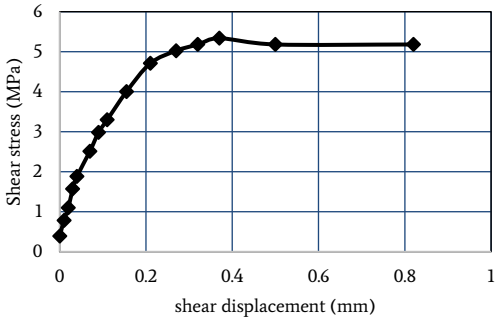

Figure 6. Shear stress - shear displacement diagram of the joint surface.

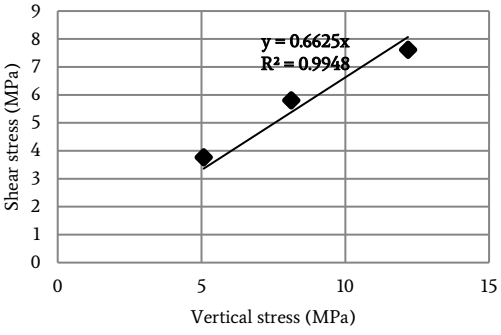

Figure 7. shear stress (τ) - vertical stress (σ_n) diagram of the joint surface.

height and width of the caving in the images of each stage were applied by AutoCAD software. In other words, in each photo, the height

Table 4. direct shear and Schmidt hammer tests results.

Properties	C_j (MPa)	φ_j	JRC	JCS (MPa)	UCS (MPa)	K_n (GPa/m)	K_s (GPa/m)	JCS
Value	0	29.5	3	71.3	37.35	38.076	14.43	71.3

Table 5. Calculated scale factors.

Quantity	Length	Density	Gravity acceleration	Modulus of elasticity	Strain	Stress	Displacement	Joint friction angle	Poisson ratio
Symbol	C_l	C_ρ	C_g	C_E	C_s	C_σ	C_δ	C_f	C_ν
Value	0.01	1	1	1	1	1	0.01	1	1

of the fall was measured by recognizing the size of the created span. The center of the blocks was painted with a color different from the background of the block. Then, the side borders were placed at a distance of one meter from each other, and their vertical position was controlled by alignment. Plexiglas was placed in front of the model. Next, the foundations of stone blocks were laid from the ground level to a height of 50 cm, followed by leveling the surface of the bases and placing travertine blocks on each of these bases. Due to the dimensions of the model (1×1.5 square meters) and travertine blocks (4×4 square centimeters) in each model, 938 blocks were needed, and picking this number of blocks in the model required extensive time. After finishing the arrangement of the blocks, the back plates were put in place. Further, the side screws were rotated to apply lateral pressure and establish a zero-displacement condition. The axis of the camera was placed at the center of the model. To create the undercut, the bases were gradually removed from the center of the model. A 4-cm undercut was created by removing each of the bases, and this process continued with the removal of all the foundations.

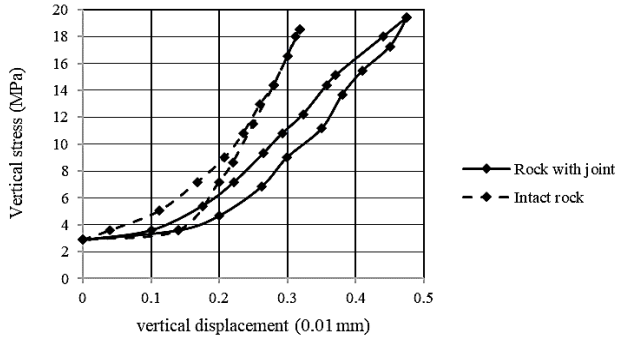

Figure 8. vertical stress - vertical displacement diagram of intact rock along with intact rock with the joint.

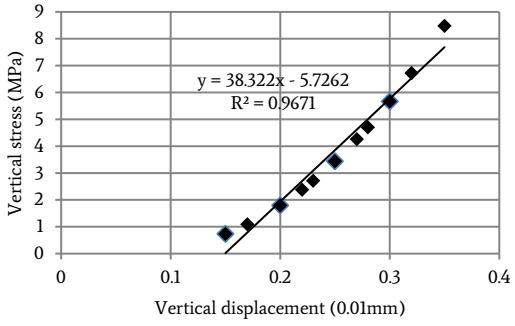

Figure 9. Vertical stress - vertical joint displacement diagram.

In the first model, a rock mass with two joint sets perpendicular to each other was simulated, which was 1.5 meters high under the weight of the block itself. In the second model, the same conditions were performed with a dip of 45 and 135. Eventually, three joint sets with a dip of 30 and 120 degrees (two joint sets intersecting with a dip of 90 degrees) and under the gravity stress of 2.5 MPa were simulated in the third model. Figures 10 and 11 depict examples of performed experiments.

5. Results and discussion

5.1. Analysis of vertical and horizontal joints test

The undercut is a space wider than the self-supported span. Also, the roof was caved after blasting and drawing the fragmented material. Considering that the creation of an undercut in a 2D model can be considered similar to the excavation of a space larger than a self-supported span, caving can be examined as an instability mechanism in this space.

In a physical model, the angle between the joints is right; therefore, the breaking state of the roof layers can be considered a broken beam. Given that the applied stress to the model is the only gravitational stress of travertine blocks, the uniaxial compressive strength of the blocks is highly greater than this stress. After the beginning of the caving mechanism, bending occurs in the roof layers. It can be considered that the mechanism of caving initiation is caused by the force of gravity because the initial horizontal stresses at the borders are extremely low. Caving propagates upwards and then stops with an increase in the span (Figure 8). In other words, in spans where caving occurs up to a certain height, the initiation and propagation of caving occur according to the definition of caving, but continuous caving is unachievable.

After the beginning of the fall, bending failure occurs in the roof layers by increasing the ratio of the beam length (the opening created by the undercut) to the distance of the joints (Figure 11).

Based on the obtained data, caving does not occur in some parts of the undercut (Figure 11, at the height of 32 cm), which has fallen over time. These results are consistent with those of Beck et al. [6] at the Ridgeway deep mine in Australia.

When the undercut is created along the entire width of the model, the bending in the layers reaches the ceiling and causes the caving to reach the total height of the model, leading to the continuous occurrence of caving. In this case, the mechanism of caving is caving resulting from settlement, because the shear strength of the rock mass at the boundaries is less than the force of gravity; moreover, slippage at the vertical boundaries of the block occurs due to the creation of a large space under the block.

Additionally, the height of the undercut does not affect the caving in this model because there is no change in the behavior of the upper layers of the roof (the broken beam). Finally, when the caving reaches the ceiling, the shape of the resulting settlement is in good agreement with the results of Vyazmensky [46]. The amount of settlement was 20 cm.

According to the obtained experiences from the double undercut with a height of 42 meters in the Northpark mine and the results from international caving studies, the undercut height does not affect the caving.

However, the height of the undercut may affect the stability of the rib pilar. In this method, the caving mechanism does not differ by increasing the height of caving (increasing the height of the undercut) in each sequence since the undercut is created sequentially. No rib pillar is left in the block caving method. At one stage of undercutting (e.g., 8 cm), the height of the undercut affects the stability of the remaining side

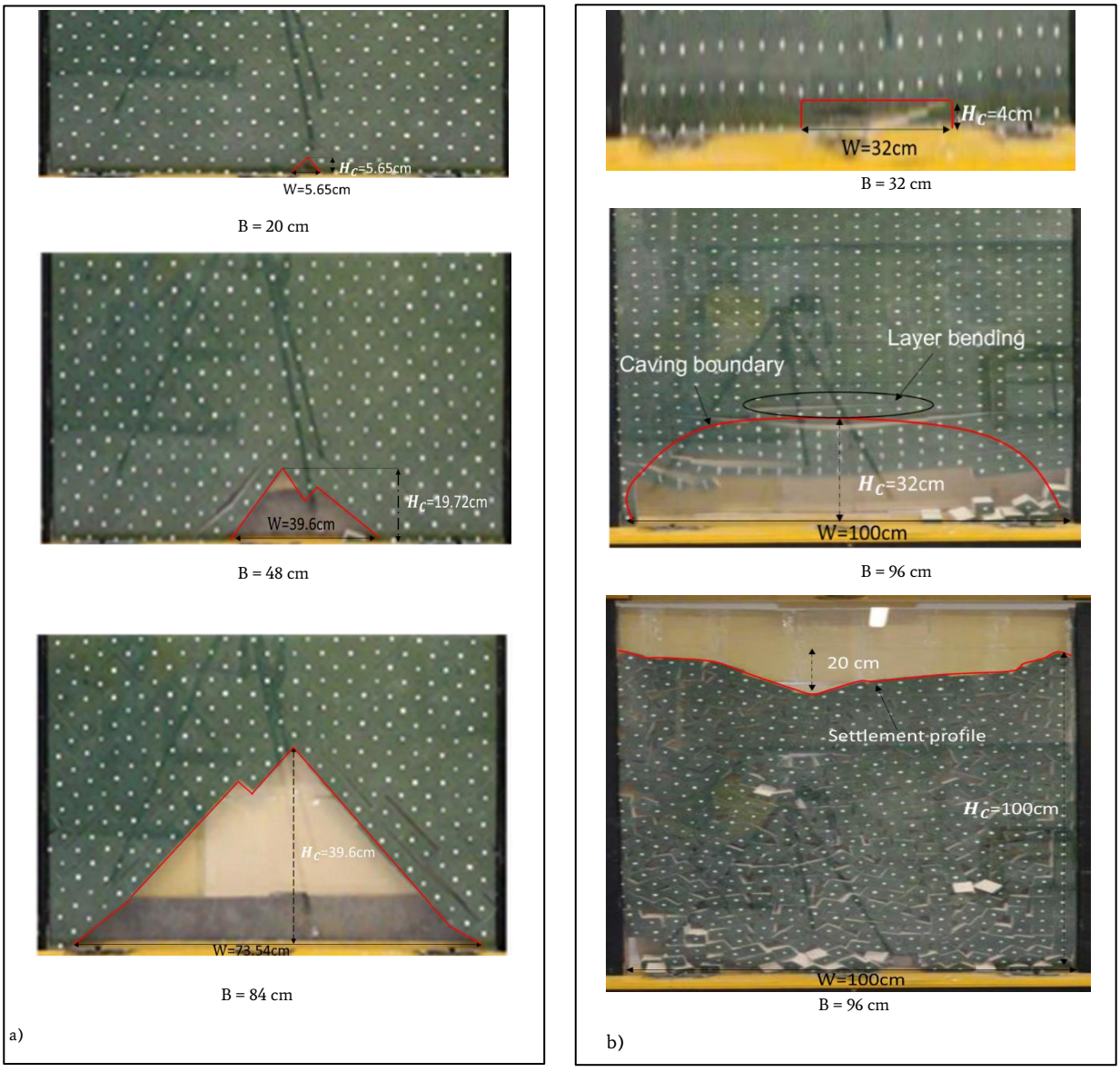

Figure 10. Examples of physical models without overburden stress: a) Dip 45- and 135-degree, b) Dip 0 and 90 degrees.

materials, but these materials are then removed to complete the undercut space. Therefore, its stability has no effect on the critical dimension.

In addition, a lack of drawing of all the fallen blocks will form a column that prevents the above blocks from falling. This can be observed from the 88-cm span on the right side of the model. In other words, if the draw control is not correctly performed, the formation of bases in the walls reduces the undercut area and affects cavability. To solve such a problem in caving mines, the rock mass boundaries are loosened by blasting. This issue highlights the importance of draw control in the caving method. Due to the almost uniform draw and a high drawing rate, the blocks have extremely little crushing when moving in the draw column.

In the 2.5 MPa overburden test, the initial caving occurs at a 12-cm span (Figure 12), which is reduced compared to the non-overburden state, where caving occurs at a 24-cm span. Furthermore, in the same spans, the height of the cave-back is higher in the presence of overburden pressure in the two models; however, the caving stops at the 44-cm span, and a stable arc is formed accordingly. Thus, the caving does not propagate upwards by an increase in the span. This is due to the difference in horizontal stress between the two models. In the case of overburden stress, the amount of horizontal stress in the model is 440 kPa, while the value of this stress is 6.61 kPa in the model without overburden stress. Therefore, horizontal stress has a positive role in caving initiation [24,27], but it locks the blocks and prevents them from falling during propagation.

As shown in Figures 13 and 14, the height and the width of the cave-back increase by increasing the span. Additionally, the height of the cave-back in the case of two joints with dips of 45 and 135 is higher than in the case of two joints with dips of 0 and 90. However, the width of the cave-back has an opposite trend. In the first case (dips 45 and 135 degrees), the span of caving initiation is smaller compared to the second case (dips 0 and 90 degrees). As the size of the span increases, the difference in the height of the cave-back in the two cases represents an increase.

Based on data in Figures 12 and 13, there is an exponential relationship between the height and width of the cave-back with the created span, and the gradient of changes in the height and width of the caving increases when the span is closer to its critical size.

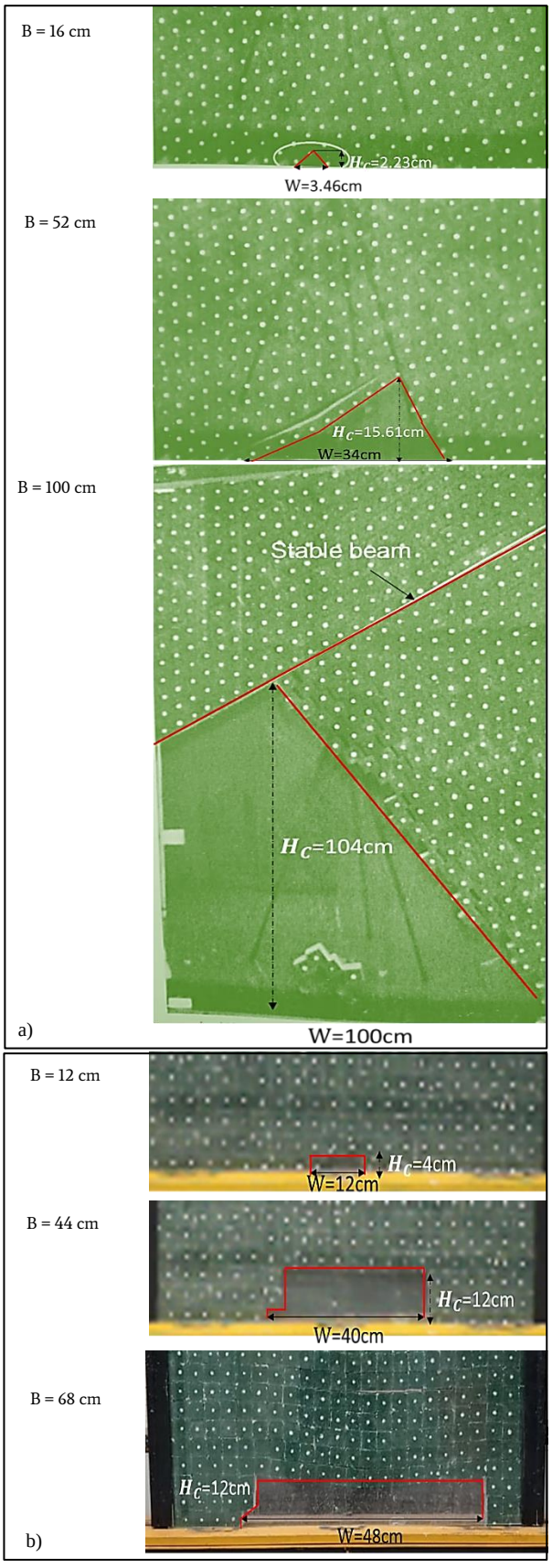

Figure 11. Examples of physical models with overburden stress: (a) Dip 30- and 120-degree, (b) Dip 0 and 90 degrees.

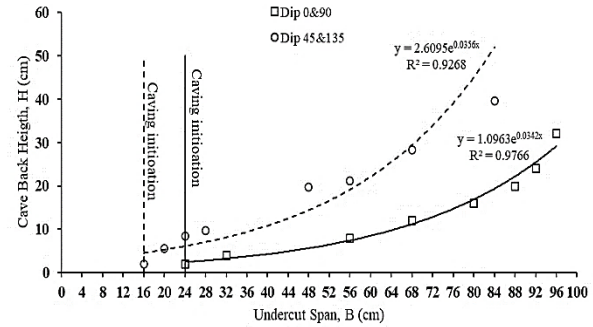

Figure 12. Cave-back height as a function of the undercut span without overburden stress.

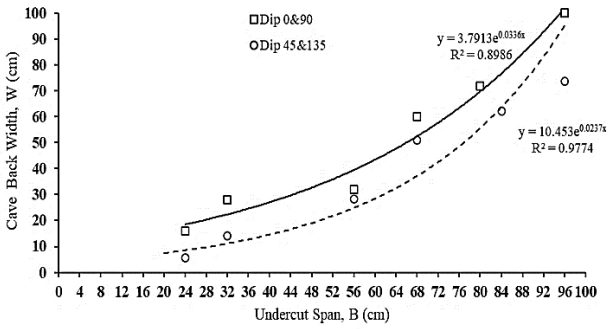

Figure 13. Cave-back width as a function of undercut span without overburden stress.

5.2. Analysis of two inclined joint sets

After placing the blocks, the lateral load was applied through the side screws, and the test was performed according to the steps mentioned earlier. In this case, the sinusoidal component of gravity is less than that of the vertical and horizontal joints, and the resistive force or the cosine component of gravity is higher than that of the vertical and horizontal joints. Therefore, in this case, the formed beams are expected to have more resistance. As depicted in Figure 8, the failure mechanism begins when the block falls from the roof of the undercut.

As the width of the undercut increases, the bending of the layers due to the increase of the undercut's span is observable (Figure 11). In addition, the locking of some blocks has prevented them from falling in some parts. The initial caving has occurred at an undercut width of 20 cm, and the shape of the fallen zone follows the dip of the joints. Hence, the behavior associated with the direction of the displacement of the rock mass at the time of the fall is controlled by the orientation of the joints.

The mechanism of caving, in this case, is subsidence caving; this is because the shear strength of the rock mass at the boundaries is less than the force of gravity, and the slip at the vertical boundaries of the block has occurred due to the creation of a large empty space under the block.

In the experiment with an overburden pressure of 2.5 MPa and a slope of 30 and 120 °, the initial caving occurs at a 12-cm span (Figure 14), which is decreased compared to the non-overburden state where the caving occurs at a 16-cm span. This issue is also related to the difference in the dip of the joints. Furthermore, in the same spans in the two models, the height of the cave-back is higher in the presence of overburden pressure. However, the caving stops at the span of 100 cm, and a stable beam is formed (Figure 9) so that the caving does not propagate upwards. This is because of the difference in horizontal stress between the two models.

Based on the findings of Figures 15 and 16, the height and the width of the cave-back increase by an increase in the span (in dips of 30 and 12 degrees). At the dip of 0 and 90 degrees, due to the presence of high horizontal stresses, the height of the cave-back does not exceed 12 cm and has not changed by the increase of the span dimension.

Moreover, the height of the cave-back in the case of two joints with dips of 30 and 120 is higher in comparison to the case of two joints with dips of 0 and 90; however, the width of the cave-back represents a reverse trend. The size of the span for caving initiation is the same in both cases. As the size of the span increases, the difference in the height of the cave-back indicates an increase in both cases.

Based on data in Figure 14, the height of the cave-back does not increase significantly by increasing the size of the undercut span, which occurs due to horizontal stresses and the vertical dip of the joints. When the joints are inclined, the height of the cave-back increases by an increase in the size of the span. In both cases, the width of the cave-back increases by increasing the span size (Figure 15).

As shown in Figures 19 and 17, the amount of the caving height has increased by increasing vertical stress. This increase is up to a certain amount of the span dimension and then the trend is constant, which is due to the presence of confining stress. The caving initiation spans for the various experiments are given in Table 6. In cases 3 and 4, the caving initiation spans are the same, but the cave-back height is 4 cm for case 3 and 2.18 cm for case 4.

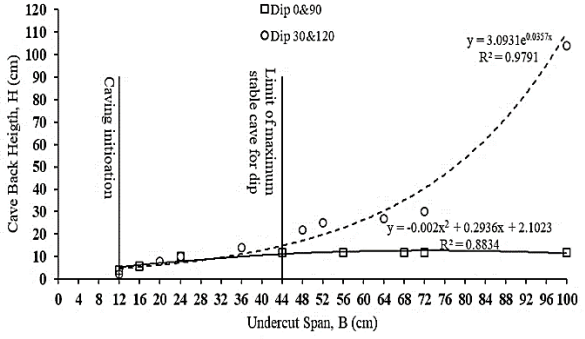

Figure 14. Cave-back height as a function of the undercut span with overburden stress.

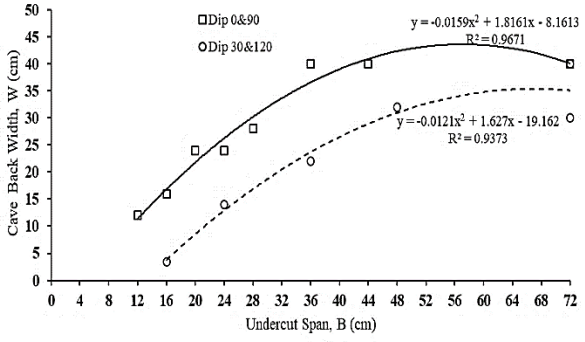

Figure 15. Cave-back width as a function of the undercut span with overburden stress.

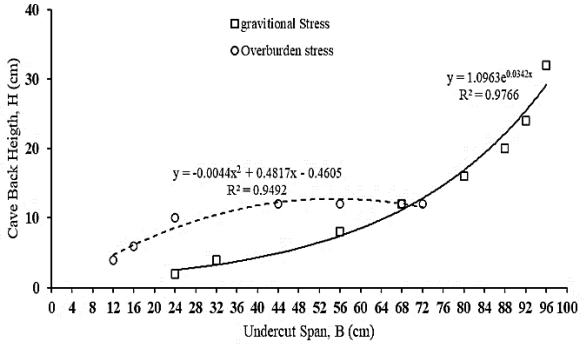

Figure 16. Cave-back height as a function of the undercut span and vertical stress.

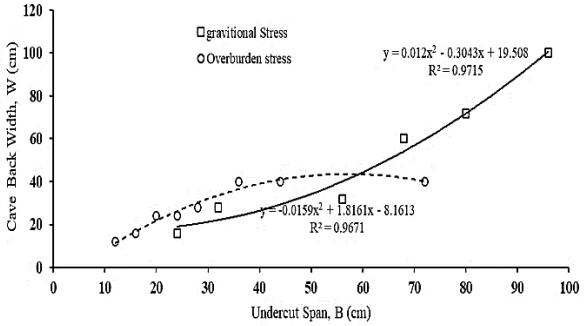

Figure 17. Cave-back width as a function of the undercut span and vertical stress.

Table 6. Caving initiation spans.

Case	initiation caving span (cm)
Case 1: 0 &90 without overburden pressure	24
Case 2: 45 &135 without overburden pressure	16
Case 3: 0 &90 with overburden pressure	12
Case 3: 30 &120 with overburden pressure	12

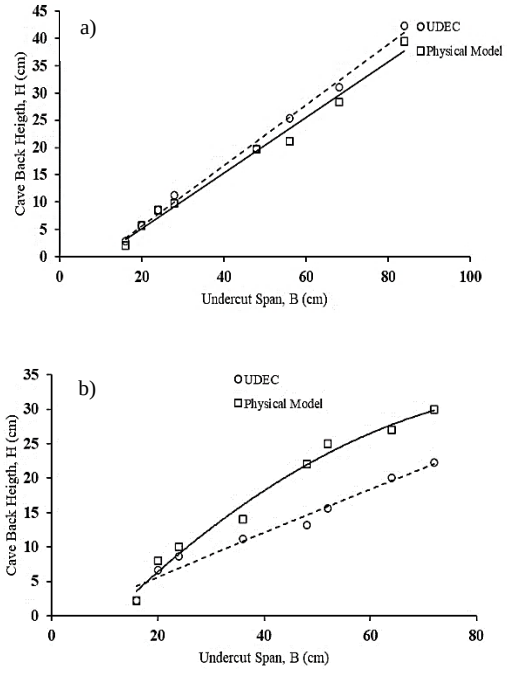

Figure 18. Comparisons of DEM simulations with physical models for various dips: (a) 45 and 135 degrees and (b) 30 and 120 degrees.
Note. DEM: Discrete element method.

6. Numerical modeling

Due to the discontinuity of the physical model, the DEM method was used for its simulation. The properties of travertine and joints (Tables 3 and 4) were included in the numerical model. According to the physical model, the model boundaries were considered limited displacements. The boundary conditions of the model walls were fixed as a roller abutment and the floor conditions of the model in both directions. Overburden pressure was applied as stress on the upper limit of the model. The dimensions of the model are the same as the physical model of 1 meter by 1.5 meters. The joints are similar to the physical model with a spacing of 4 cm in the model.

Similar to the physical model, fallen blocks are allowed to exit the model floor. The dimensions of the mesh were changed from 4 cm to

0.5 cm, and it was observed that the results did not change from 2 cm smaller. Therefore, the optimal mesh dimensions of 2 cm were considered for this purpose. Based on the results of the uniaxial compressive test, the blocks were in the elastic state, thus in the numerical model, the elastic behavioral and Mohr-Columb behavioral models were used for the blocks and joints, respectively. According to the modeling process, first, the model was balanced with elastic behavior, and then the behavioral model of the joints was changed to Mohr-Columb, and the undercut was created accordingly. In addition, the amount of the friction angle between the steel and stone was applied at the lateral boundaries of the numerical model. Similar to the physical model, a 4-cm undercut was created in each step in the numerical model.

In the numerical model, caving is created in the upper layers of the undercut. The UDEC results are compared with those of the physical models in Figures 17 and 18 for various dips of vertical stresses. Figure 19 illustrates examples of UDEC models after caving for various spans and dips. Figure 20 displays the strain contour at the corresponding spans in Figure 19. As shown in Figure 20, the shape of the caving zone follows that of the strain zone.

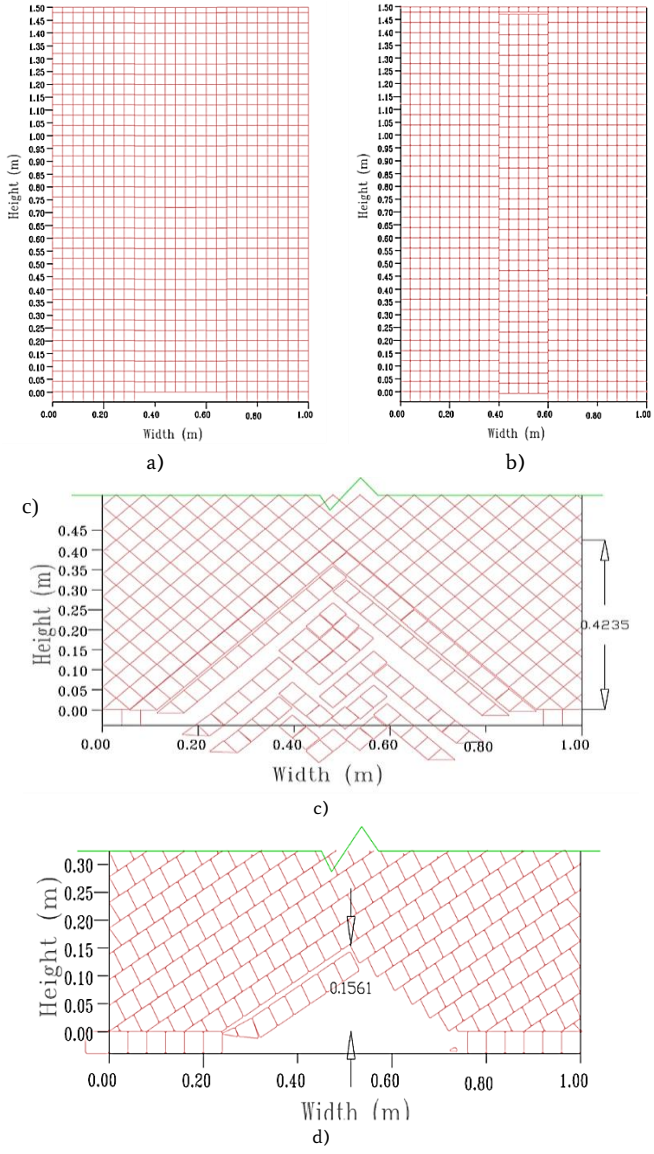

Figure 19. DEM simulation results for different dips: (a) 0 and 90 degrees without overburden stress, (b) 0 and 90 degrees with overburden stress, (c) 45 and 135 degrees without overburden stress, and (d) 30 and 120 degrees with overburden stress. *Note.* DEM: Discrete element method.

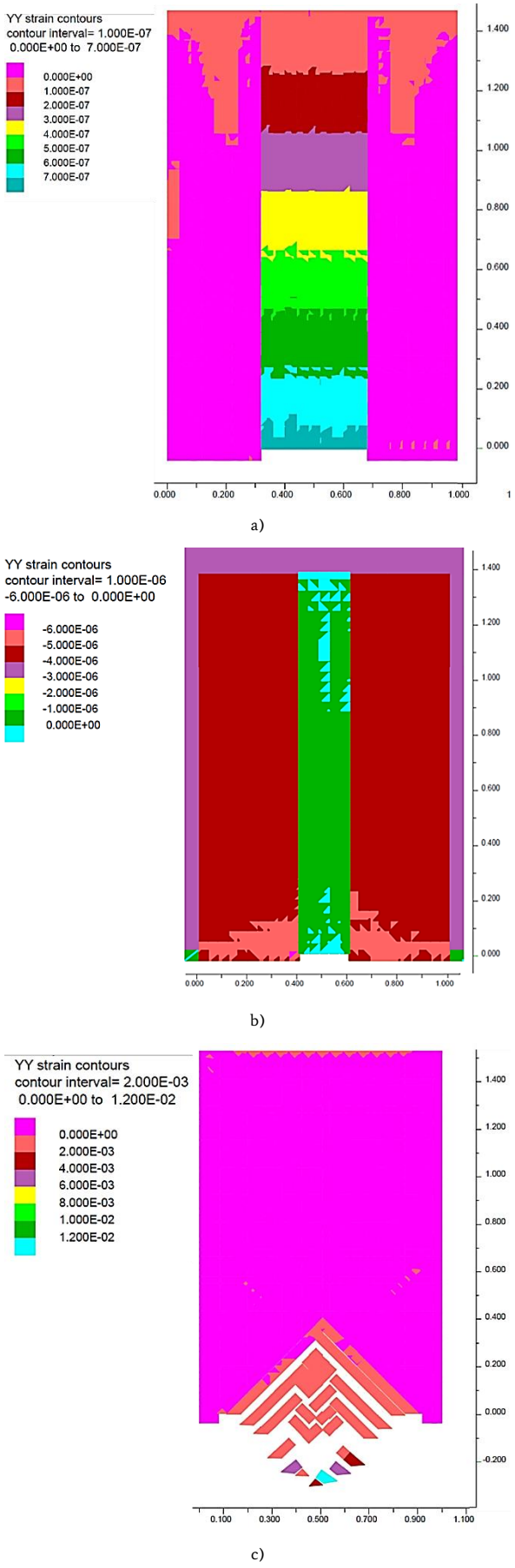

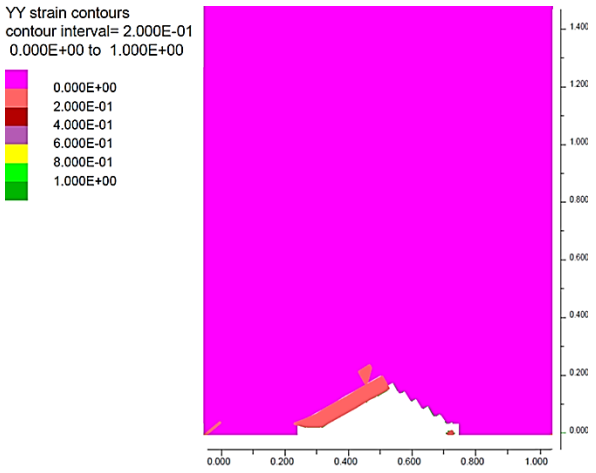

Figure 20. Strain contours for different dips: (a) 0 and 90 degrees without overburden stress, (b) 0 and 90 degrees with overburden stress, (c) 45 and 135 degrees without overburden stress, and (d) 30 and 120 degrees with overburden stress.

7. Conclusions

The current study attempted to analyze jointed rock mass behavior in the block caving method by physical and numerical modeling. The image analysis method was used to measure the height of the caving in the physical model. According to the results, the failure mechanism in both cases of vertical and horizontal joints was bending in the roof layers. The results also showed that the height of the undercut did not affect cavability, because there was no change in the behavior of the upper layers of the roof by increasing the height of the undercut. The importance of draw control as a critical parameter in the propagation of caving was another finding of this research. In the physical model, it was observed that if the draw control is not done correctly, the formation of pillars in the walls will reduce the undercut area, and the process will be challenging. Moreover, it was found that in the physical model, if the lateral pressure is more than a certain amount, so as not to overcome the strength of the rock, it may cause locking in the stone blocks and propagation in the process. In the case of overburden pressure, the minimum caving initiation span is reduced from 24 to 12 cm (in the case of 0 and 90 ° joints). Furthermore, in the same span, the height of the caving in the presence of overburden is nearly 40% higher. Based on the findings, the width of the caving area increased by increase in the overburden pressure by 10%. In the case of an inclination joint, the minimum caving span was 50% of the horizontal and vertical joints.

Acknowledgments

Physical modeling has been done at the rock mechanics laboratory of the university of Tehran and thanks to all of the relevant authorities.

REFERENCES

[1]. Laubscher, D. (2000). Cave Mining Handbook.

[2]. Chitombo, G. P. (2010). Cave mining: 16 years after Laubscher's 1994 paper gave mining–state of the art'. Mining Technology, 119(3), 132-141.

[3]. Rice, G. S. (1934). Ground movement from mining in Brier Hill mine, Norway, Michigan. Mining and Metallurgy, 15(325), 12-14.

[4]. Panek, L. A. (1984). Subsidence in undercut-cave operations, subsidence resulting from limited extraction of two neighboring-cave operations. Geomechanical applications in hard rock mining, 225-240.

[5]. Carlson, G., and Golden, R. (2008, June). Initiation, Growth, Monitoring, and Management of the 7210 Cave at Henderson Mine-A case study. In 5th International Conference and Exhibition on Mass Mining (Vol. 9, pp. 97-106).

[6]. Beck, D., Sharrock, G., and Capes, G. (2011). A coupled DFE-Newtonian cellular automata scheme for simulation of cave initiation. In Propagation and Induced Seismicity. 45th US Rock Mechanics/Geomechanics Symposium Held in San Francisco, CA.

[7]. Someehneshin, J., Oraee-Mirzamani, B., and Oraee, K. (2015). Analytical model determining the optimal block size in the block caving mining method. Indian Geotechnical Journal, 45(2), 156-168.

[8]. Mahtab, M. A., and Dixon, J. D. (1976). Influence of rock fractures and block boundary weakening on cavability. Trans Soc Min Eng AIME, 260(1), 6-12.

[9]. McMahon, B. K., and Kendrick, R. F. (1977). Predicting the block caving behavior of orebodies. Society of Mining Engineers of AIME.

[10]. Carter P. G. (2011). Selection Process for Hard Rock Mining. SME mining engineering Handbook (Vol. 1). SME.

[11]. Laubscher, D. H. (1990). A geomechanics classification system for the rating of rock mass in mine design. Journal of the Southern African Institute of Mining and Metallurgy, 90(10), 257-273.

[12]. Mawdesley, C., Trueman, R., and Whiten, W. J. (2001). Extending the Mathews stability graph for open–stope design. Mining Technology, 110(1), 27-39.

[13]. Stewart, S. B. V., and Forsyth, W. W. (1995). The Mathew's method for open stope design. CIM Bulletin, 88(992), 45-53.

[14]. Trueman, R., Mikula, P., Mawdesley, C. A., and Harries, N. (2000). Experience in Australia with the application of the Mathew's method for open stope design. The CIM Bulletin, 93(1036), 162-167.

[15]. Mawdesley, C. A. (2002). Predicting rock mass cavability in block caving mines.

[16]. Tollenaar, R. N. (2008). Characterization of discrete fracture networks and their influence on caveability and fragmentation (Doctoral dissertation, University of British Columbia).

[17]. Lorig, L. J., Board, M. P., Potyondy, D. O., and Coetzee, M. J. (1995, October). Numerical modelling of caving using continuum and micro-mechanical models. In Proc. of CAMI'95 Canadian Conference on Computer Applications in the Mining Industry, Montreal, Quebec, Kanada (pp. 416-424).

[18]. Brown, E T. (2003). Block Caving Geo-mechanics. The International Caving Study I. JKMRC Monograph Series in Mining and Mineral Processing 3. University of Queensland.

[19]. Gilbride, L. J., Free, K. S., and Kehrman, R. (2005, June). Modeling Block Cave Subsidence at the Molycorp, Inc., Questa Mine? A Case Study. In Alaska Rocks 2005, The 40th US Symposium on Rock Mechanics (USRMS). OnePetro.

[20]. Kalenchuk, K. S., McKinnon, S., and Diederichs, M. S. (2008). Block geometry and rock mass characterization for prediction of dilution potential into sub-level cave mine voids. International Journal of Rock Mechanics and Mining Sciences, 45(6), 929-940.

[21]. Xie, Y. S., and Zhao, Y. S. (2009). Numerical simulation of the top coal caving process using the discrete element method. International Journal of Rock Mechanics and Mining Sciences,

46(6), 983-991.

[22]. Sharrock, G., Vakili, A., Duplancic, P., and Hastings, N. (2011). Numerical analysis of subsidence for Perserverence Deeps Block Cave in Continuum and Distinct Element Numerical Modelling in Geomechanics. Sainsbury, Hart, Detournay, and Nelson (eds.), Paper, 06-03.

[23]. Gao, F., Stead, D., and Coggan, J. (2014). Evaluation of coal longwall caving characteristics using an innovative UDEC Trigon approach. Computers and Geotechnics, 55, 448-460.

[24]. Rafiee, R., Ataei, M., KhalooKakaie, R., Jalali, S. E., Sereshki, F., and Noroozi, M. (2018). Numerical modeling of influence parameters in cavabililty of rock mass in block caving mines. International Journal of Rock Mechanics and Mining Sciences, 105, 22-27.

[25]. Song, Z., and Konietzky, H. (2019). A particle-based numerical investigation on longwall top coal caving mining. Arabian Journal of Geosciences, 12(18), 1-18.

[26]. Wang, J., Wei, W., Zhang, J., Mishra, B., and Li, A. (2020). Numerical investigation on the caving mechanism with different standard deviations of top coal block size in LTCC. International Journal of Mining Science and Technology, 30(5), 583-591.

[27] Alipenhani, B., Majdi, A., and Bakhshandeh Amnieh, H. (2022). Determination of caving hydraulic radius of rock mass in the block caving method using numerical modeling and multivariate regression. Journal of Mining and Environment, doi.org/10.22044/jme.2022.11589.2149

[28]. Park, D. W., and Kicker, D. C. (1985). Physical model study of a longwall mine. Mining Science and Technology, 3(1), 51-61.

[29]. Kang, H., Li, J., Yang, J., and Gao, F. (2017). Investigation on the influence of abutment pressure on the stability of rock bolt reinforced roof strata through physical and numerical modeling. Rock Mechanics and Rock Engineering, 50(2), 387-401.

[30]. McNearny, R. L., and Abel Jr, J. F. (1993, April). Large-scale two-dimensional block caving model tests. In International Journal of rock mechanics and mining sciences and geomechanics abstracts (Vol. 30, No. 2, pp. 93-109). Pergamon.

[31]. Carmichael. P. and Hebblewhite. B. (2012). An investigation into semi-intact rock mass representation for physical modelling block caving mechanics zone. Mining education Australian Research projects review.

[32]. Cumming-Potvin, D., Wesseloo, J., Jacobsz, S. W., and Kearsley, E. (2016). Results from physical models of block caving. In 7th International Conference and Exhibition on Mass Mining (MassMin 2016), 9-11 May 2016, Sydney, New South Wales, Australia (pp. 329-340). Australasian Institute of Mining and Metallurgy.

[33]. Jacobsz, S. W., Kearsley, E. P., Cumming-Potvin, D., and Wesseloo, J. (2018, July). Modelling cave mining in the geotechnical centrifuge. In Physical Modeling in Geotechnics, The 9th International Conference on Physical Modelling in Geotechnics (ICPMG 2018) (pp. 809-814).

[34]. Bai, Q., Tu, S., and Wang, F. (2019). Characterizing the top coal cavability with hard stone band (s): insights from laboratory physical modeling. Rock Mechanics and Rock Engineering, 52(5), 1505-1521.

[35]. Heydarnoori, V., Khosravi, M. H., and Bahaaddini, M. (2020). Physical modelling of caving propagation process and damage profile ahead of the cave-back. Journal of Mining and Environment, 11(4), 1047-1058.

[36]. Rafiee, R., Ataei, M., KhaloKakaie, R., Jalali, S. E., and Sereshki, F. (2016). A fuzzy rock engineering system to assess rock mass cavability in block caving mines. Neural Computing and Applications, 27(7), 2083-2094.

[37]. Azadmehr, A., and Jalali, S. M. E. (2017). Assessment of rock mass caveability in block caving mining method, using Rock Engineering Systems (RES). Tunneling and Underground Space Engineering, 6(1), 57-78.

[38]. Rafiee, R., Ataei, M., Khalokakaie, R., Jalali, S. M. E., and Sereshki, F. (2015). Determination and assessment of parameters influencing rock mass cavability in block caving mines using the probabilistic rock engineering system. Rock Mechanics and Rock Engineering, 48(3), 1207-1220.

[39]. Mohammadi, S., Ataei, M., Kakaie, R., Mirzaghorbanali, A., and Aziz, N. (2021). A Probabilistic Model to Determine Main Caving Span by Evaluating Cavability of Immediate Roof Strata in Longwall Mining. Geotechnical and Geological Engineering, 39(3), 2221-2237.

[40]. Castro, R., Gómez, R., Pierce, M., & Canales, J. (2020). Experimental quantification of vertical stresses during gravity flow in block caving. International Journal of Rock Mechanics and Mining Sciences, 127, 104237.

[41]. Bahaaddini, M., Sharrock, G., Hebblewhite, B. K., & Mitra, R. (2012, June). Direct shear tests to model the shear behavior of rock joints by PFC2D. In 46th US Rock Mechanics/Geomechanics Symposium. OnePetro.

[42]. Bandis, S. C., Lumsden, A. C., & Barton, N. R. (1983, December). Fundamentals of rock joint deformation. In International Journal of Rock Mechanics and Mining Sciences & Geomechanics Abstracts (Vol. 20, No. 6, pp. 249-268). Pergamon.

[43]. Brady, B. H., & Brown, E. T. (2006). Rock mechanics: for underground mining. Springer Science & Business Media.

[44]. Weishen, Z., Yong, L., Shucai, L., Shugang, W., & Qianbing, Z. (2011). Quasi-three-dimensional physical model tests on a cavern complex under high in-situ stresses. International Journal of Rock Mechanics and Mining Sciences, 48(2), 199-209.

[45]. Fuenkajorn, K., & Phueakphum, D. (2010). Physical model simulation of shallow openings in jointed rock mass under static and cyclic loadings. Engineering Geology, 113(1-4), 81-89.

[46]. Vyazmensky, A., Elmo, D., and Stead, D. (2010). Role of rock mass fabric and faulting in the development of block caving induced surface subsidence. Rock mechanics and rock engineering, 43(5), 533-556.